ANCHOR: A Technical Approach to Monitor Single-Copy Locus Localization in Planta

Anis Meschichi, Mathieu Ingouff, Claire Picart, Marie Mirouze, Sophie Desset, Franck Gallardo, Kerstin Bystricky, Nathalie Picault, Stefanie Rosa, Frédéric Pontvianne

ANCHOR, a technical approach to monitor single-copy locus localization *in planta*

Anis Meschichi[1]*, Mathieu Ingouff[2]*, Claire Picart[3] Marie Mirouze[2,4], Sophie Desset[5] , Franck Gallardo[6], Kerstin Bystricky[7], Nathalie Picault[3], Stefanie Rosa[1], Frédéric Pontvianne[3]#

[1] Swedish University of Agricultural Sciences, Uppsala, Sweden.
[2] Université de Montpellier, DIADE, Montpellier, France.
[3] CNRS, Laboratoire Génome et Développement des Plantes (LGDP), Université de Perpignan Via Domitia, Perpignan, France.
[4]Institut de Recherche pour le Développement, DIADE, Montpellier, France.
[5] CNRS, GReD, Université Clermont Auvergne, INSERM, BP 38, 63001 Clermont–Ferrand, France.
[6] NeoVirTech SAS, 1 Place Pierre Potier, 31000 Toulouse, France.
[7] Laboratoire de Biologie Moléculaire Eucaryote (LBME), Centre de Biologie Intégrative (CBI), CNRS, UPS, University of Toulouse, 31062, Toulouse, France.

*equal contribution
#corresponding author

RESUME

Together with local chromatin structure, gene accessibility and the presence of transcription factors, gene positioning is implicated in gene expression regulation. Although the basic mechanisms are expected to be conserved in eukaryotes, little is known about the role of gene positioning in plant cells, mainly due to the lack of a highly resolutive approach. In this manuscript, we adapted the use of the ANCHOR system to perform real-time single-locus detection *in planta*. ANCHOR is a DNA-labelling tool derived from the chromosome partitioning system presents in many bacterial species. We demonstrate its suitability to monitor a single-locus *in planta* and used this approach to track chromatin mobility during cell differentiation in *Arabidopsis thaliana* root epidermal cells. Finally, we discuss the potential of this approach to investigate the role of gene positioning during transcription and DNA repair in plants.

INTRODUCTION

In Eukaryotes, genetic information is encoded in the chromatin, a complex structure composed of DNA packed around an octamer of histones in the nucleus. Chromosome territories form large compartments in the nucleus, themselves containing chromatin domains harbouring different epigenetic signatures (Santos et al., 2020; Pontvianne and Grob, 2020; Nguyen and Bosco, 2015). In these domains, the positioning and accessibility of genes are very dynamic in response to several key biological processes that include gene transcription, genome replication and DNA repair for example. Fluorescence *in situ* Hybridization (FISH) approaches such as padlock-FISH enable to detect a single-copy locus using fixed plant material (Feng et al., 2014). However, imaging techniques using non-living organisms is insufficient to track spatial and temporal dynamics of loci. Live-cell imaging approaches allow gene positioning visualization during these different processes, providing key elements for their understanding (Shaban and Seeber, 2020; Dumur et al., 2019).

Microscopic detection of genomic loci in plants is possible through the use of different strategies including zinc-finger based imaging, transcription activator–like effectors (TALE) and CRISPR/Cas9 (Khosravi et al., 2020; Fujimoto et al., 2016; Lindhout et al., 2007). Unfortunately, these techniques have been restricted to follow the dynamics of highly repeated regions

(centromeric repeats, telomeric sequences and ribosomal RNA genes). Monitoring of a single locus in living plants is possible thanks to the addition of *lacO* motifs to which the transcription factor LacI, fused to a fluorescent protein, can bind (Fang and Spector, 2007; Kato and Lam, 2003). Live-cell imaging of *FLOWERING LOCUS C* (*FLC*) alleles associated to *lacO* (*FLC-LacO)* could be performed to demonstrate that *FLC-LacO* repression during vernalization provokes their physical clustering (Rosa et al., 2013). In addition, the Tet repressor protein fused to a fluorescent protein could also be used to label a genomic region containing numerous Tet operator sequences (Matzke et al., 2005). In both cases, amplification of the signal is directly linked to the multiplicity of the targeted sequences. However, these repetitions often affect local chromatin organization and can trigger silencing of the reporter gene (Watanabe et al., 2005). Thus, a standardized and robust technique for tracking the dynamic of a single locus is still not available.

The ANCHOR system is a DNA-labeling tool derived and optimized from chromosome partitioning complex of bacteria. A single-copy of *parS* -1 kb long fragment- serves as a binding platform for ParB proteins (Dubarry et al., 2006). Natural *ParS* sequence is composed of 4 canonical inverted repeat sequences that are bound via the helix-turn-helix (HTH) motif present in ParB (Funnell, 2016). Upon binding, oligomerization of ParB proteins then propagates over the *ParS* sequence and adjacent DNA (Figure 1A). Importantly, oligomerized ParB are loosely associated and can be displaced transiently and easily upon transcription or DNA repair (Saad et al., 2014). This phenomenon is also described as the caging step (Funnell, 2016). This system has been adapted successfully to monitor a unique locus in living yeast and human cells using a fluorescent-tagged ParB (Germier et al., 2017). This approach is also able to visualize DNA viruses in human cells (Gallardo et al., 2020; Mariamé et al., 2018; Komatsu et al., 2018; Blanco-Rodriguez et al., 2020; Hinsberger et al., 2020). In this manuscript, we demonstrate that the ANCHOR system can also be used to visualize a single-locus in fixed and living plant tissues. Using this approach, we also show that chromatin mobility is different in differentiated cells compared to meristematic cells of plants.

MATERIAL AND METHODS

Plant Materials and Growth Conditions

Arabidopsis thaliana ecotype Col-0 was used in this study. *lacO*/LacI line used comes from the following source (Matzke et al., 2005). To test the ANCHOR system, *Arabidopsis thaliana* (Col-0) plants were transformed by agroinfiltration using the floral dip protocol (Clough and Bent, 1998), using *Agrobacterium tumefaciens* GV3101 strain. Transformants were grown on soil and sprayed with Basta herbicide for selection (10 mg/L). All the plant material used here was grown in control growth chambers on soil at 21°C with a daylight period of 16 hr/day. The transformant 2F (T2F) line was crossed to Col-0 wild-type plants expressing the histone variant H2A.W fused to red fluorescent protein (RFP) (Yelagandula et al., 2014). The T2F line used in this study is heterozygote for the ANCHOR transgene, except in the data presented in (Figure 2), where homozygous lines have been used.

For i*n vitro* growth, seeds were surface sterilized in 5% v/v sodium hypochlorite for 5 min and rinsed three times in sterile distilled water. Seeds were stratified at 4°C for 48 h in the darkness and plated on Murashige and Skoog (MS) medium. Seedlings were placed in a growth cabinet (16 hours light, 22°C) for 1 week in vertically oriented Petri dish before imaging.

Plasmid construction

A cassette allowing the expression of ParB has been synthetized by Genescript®. The nature and sequences of the ANCHOR system are confidential and the property of NeoVirTech SAS. The cassette was cloned into the pEarleyGate302 vector (Earley et al., 2006).

Nanopore sequencing

Genomic DNA preparation was performed as previously described in (Picart-Picolo et al., 2020). Library preparation was performed using the 1D Genomic DNA by ligation kit SQK-LSK109 (Oxford Nanopore Technologies), following the manufacturer's instructions. The R9.5 ONT flow-cell FLO-MIN106D (Oxford Nanopore Technologies) was used. We obtained 1.93 Gb of sequences (11X coverage) with an average read length of 3, 675kb for ANCHOR T2F line. ONT reads mapping the transgene were mapped, filtered and aligned using Geneious® software (Kearse et al., 2012).

Cytogenetic Analyses

For cytogenetic analyses, nuclei were isolated from 3- or 4-week-old plants as previously described (Pontvianne et al., 2012). Briefly, fresh leaves were fixed in 4% formaldehyde in Tris buffer (10 mM Tris-HCL at pH 7.5, 10 mM EDTA, 100 mM NaCl) for 20 min, then chopped with a razor blade in 0.5 mL of LB01 buffer (15 mM Tris-HCl at pH 7.5, 2 mM NaEDTA, 0.5 mM spermine, 80 mM KCl, 20 mM NaCl, 0.1% Triton X-100). The lysate was filtered through a 30-µm cell strainer (BD Falcon), and 12 µL of sorting buffer (100 mM Tris-HCl at pH 7.5, 50 mM KCl, 2 mM MgCl2, 0.05% Tween-20, 5% sucrose) was added per 3 µL of cell/nuclei suspension (Pontvianne et al., 2012), and spread on a polylysine slide. After air drying, samples were post-fixed in 2% formaldehyde in Phosphate Buffer (PBS) for 5 minutes and then washed twice with water before being air-dried. Slides were then mounted in Vectashield at 1 µg/ml of DAPI and seal them with nail polish.

Nuclei with different levels of ploidy were isolated as described in (Pontvianne et al., 2016), except that propidium iodide was used to stain the nuclei, together with RNase to a final concentration of 10 µg/ml. A S3 cell sorter (Biorad®) with 488nm and 561nm 100 mW dual-lasers was used to sort the nuclei. Immunolocalization experiments were performed as described previously (Durut et al., 2014) using anti-H3K27me3 or anti-H3Ac antibodies (Abcam) to a 1/1000 dilution. Zeiss LSM 700 confocal was used to generate images presented in (Figure 1), while Zeiss LSM 800 with an Airyscan module was used to generate images from (Figure 2), (Figure 3) and (Figure 4A) with a 63x objective, N.A. 1.4 and pixel size 0.028x0.028x0.160 μm^3. Live-cell imaging presented in (Figure 4B) were performed using a spinning disk Zeiss Cell observer equipped with a high-speed Yokogawa CSUX1spinning disk confocal, an ORCA-flash 4.0 digital camera (Hamamatsu) and a ×40 water objective N.A. 1.2. Green Fluorescent Protein (GFP) was excited at 488 nm.

Live-cell Imaging

In (Figure 5), time-lapse imaging of *Arabidopsis thaliana* roots has been carried out using a Zeiss LSM 780 confocal microscope using a 63x water immersion objectives (1.20 NA). For visualization of root cell contours stained with propidium iodide, an excitation line of 488 nm was used and signal was detected at wavelengths of 580 to 700nm. For observation of GFP expression, we used respectively a 488-nm excitation line and a BP filter of 505-550 nm. For all experiments, images were acquired every 6 s taking a series of 3 optical sections with Z-step of 2 µm for 5 min. Each movie has a format of 512 × 512 pixels and a 3× zoom factor.

The 7-d-old seedlings were mounted in water, or propidium iodide, between slide and cover slip and sealed with 0.12-mm-thick SecureSeal Adhesive tape (Grace Bio-Labs), to avoid root movements and drying during imaging.

Mean square displacement analysis

All the movies have been analysed with Fiji software (NIH, Bethesda, MD, http://rsb.info.nih.gov/ij/) and with the plugin SpotTracker 2D (obtained from http://bigwww.epfl.ch/sage/soft/spottracker). Mean square displacement (MSD) analysis was performed as described in (Meschichi and Rosa, 2021). All quantitative measurements represent averages from at least 9 cells. From the MSD plot, we calculated the radius of constraint by the square root of the plateau of the MSD curve multiplied by 5/4. Data-sets where tested for normality using the Shapiro-Wilks test. Parametric analyses were done with the standard Student's *t* test to determine the statistical significance of results. For statistical analysis, we used the GraphPad Prism 8.3 software.

RESULTS

Development of the ANCHOR system

Our goal was to adapt and facilitate the use of the ANCHOR system in plants. We therefore combined the two elements of the ANCHOR system (ParB and its target sequence *parS*) into a single transgene. A *ParB* gene whose coding sequence has been optimized for *Arabidopsis thaliana* was fused in frame to a GFP and triple FLAG-tag (ParB:GFP:3XFLAG) to allow detection in living and fixed nuclei (Figure 1B). *ParB:GFP:3XFLAG* expression was placed under the control of a promoter allowing ubiquitous expression. At the 3' end of the ParB construct, we added the 1kb-long ParB target sequence *parS* separated by a 1.5 kb-long spacer sequence to prevent potential interference of *ParB* gene transcriptional activity. Such design allows rapid selection of transgenic plants containing the two linked ANCHOR elements. In addition, detection of *parS*-ParB:GFP signals would suggest that *ParB:GFP* transcription is possible even in the event of local caging of ParB:GFP proteins.

Wild-type Col-0 plants were transformed with the transgene and selected using Basta herbicide by spray. Fixed nuclei isolated from eight different T1 transformants revealed the presence of *parS*-ParB:GFP foci in five of them (Figure 1C). To test the robustness of the detection approach, we then analysed the entire root-tip from one ANCHOR line comprising a single copy insertion at generation T2 (T2F; Figure 1D). One *parS*-ParB:GFP signal was detectable in almost all nuclei analysed. Importantly, the signal-to-noise ratio is high, which allows easy detection of the specific signal (Figure 1D).

To further characterize the ability of the ANCHOR system to follow a single-locus *in planta*, it is important to know the exact location of the transgene. We performed long-read Nanopore sequencing on an ANCHOR line with one single insertion (T2F), and extracted all long reads corresponding to the transgene to map its location in the genome. Sequence analyses revealed that the transgene could be located on the lower arm of chromosome 5, at position 23 675 998 bp, in an intergenic region (Figure 1E). This position is flanked by a region enriched in active chromatin marks and a region enriched with Histone 3 trimethylated Lysine 27 (H3K27me3), a repressive mark deposit by the Polycomb repressive complex 2 (PRC2) (Figure S1) (Sequeira-Mendes et al., 2014).

Detection of *parS*-ParB *foci* in fixed cells

As presented in (Figure 1D), one unique focus was usually detected in root tip cells, sometimes appearing as a doublet. Because the ANCHOR system is based on protein aggregation, we wondered whether analysing ANCHOR signals in endoreplicated cells would lead to an increase number of detected foci. We isolated 2C , 4C and 16C cells by fluorescent-assisted cell sorting after propidium iodide labelling and RNAse treatment. We stained sorted nuclei with DAPI and observed *parS*-ParB:GFP signals in sorted nuclei. We could see an higher amount of *parS*-ParB:GFP signals in sorted nuclei presenting a higher endoreplication rate (Figure 2A and S2A). Although these data suggest that the ANCHOR system is suitable to detect multiple loci simultaneously, additional experiments are required to fully demonstrate that this reporting system does not lead to aberrant locus aggregation.

In the T2F line, the transgene is located on an arm of the chromosome 5, in a region enriched in H3K27me3 deposited by the PRC2, but flanked by a genomic region enriched with active chromatin marks (Figure S1). Although T-DNA transgene insertion may affect locally this peculiar chromatin environment (Rajeevkumar et al., 2015), we tested the possibility to combine both immunostaining and *parS*-ParB:GFP signals detection. Immunostaining experiments were performed on isolated leaf nuclei from 3-week-old plants using either an antibody against Histone 3 acetylated (H3Ac) active mark or H3K27me3 repressive mark. As expected, the tested histone marks and *parS*-ParB:GFP signals are excluded from heterochromatic foci stained by DAPI and corresponding to the centromeric, pericentromeric and nucleolus organizer regions (Figures 2B-C). Although no clear overlap could be detected between *parS*-ParB:GFP signals and H3K27me3 marks, at least partial overlap can be seen between *parS*-ParB:GFP signals and H3Ac marks (Figures 2B-C and S4). This result is expected since active transcription is necessary to produce ParB:GFP proteins. Although we cannot conclude about the specific chromatin state surrounding the transgene insertion site in T2F, this experiment demonstrate our ability to detect *parS*-ParB:GFP signals and immunodetection approach simultaneously.

Detection of *parS*-ParB *foci* in live-cell imaging

Previous studies demonstrated that global genome organisation can be cell specific and vary during plant development (Pontvianne and Liu, 2019). We therefore tested our ability to detect *parS*-ParB:GFP signals in different cell-types, directly *in planta*. To allow simultaneous visualization of heterochromatin and *parS*-ParB:GFP signals directly in living cells, we crossed the T2F line with another *A. thaliana* Col-0 line expressing the Histone 2A variant H2A.W, fused to the Red Fluorescent Protein (RFP) (Yelagandula et al., 2014). Plants were grown on MS media directly in petri dish compatible with confocal imaging. We analysed several tissues, including meristematic and differentiated root cells, leaf cells, trichome cells, but also pollen grains from plant grown on soil. We were able to detect *parS*-ParB:GFP signals in all cell-types tested (Figure 3 and S3). As expected, *parS*-ParB:GFP signals are excluded from heterochromatin area, labelled by H2A.W:RFP signals. Note that in certain cell-types, the nuclear area can be seen due to non-associated ParB proteins that are diffusing in the nucleoplasm.

The ANCHOR system does not require high DNA accessibility to allow *parS*-ParB:GFP signals visualization. In a highly condensed chromatin context like during mitosis, we could still detect *parS*-ParB:GFP signals in condensed chromosomes, although signal is usually less bright than in the neighboring cells (Figure 4A).

Finally, we tested our ability to perform live-cell imaging of the *parS*-ParB:GFP signals *in planta*. We analysed *parS*-ParB:GFP dynamics in living roots using a Zeiss Cell Observer Spinning

disk microscope (Figure 3B). Although bleaching can alter the signal detection over time, we were able to detect the ParB:GFP signals at multiple time points and track its relative nuclear position, as previously reported in human and yeast cells (Saad et al., 2014; Germier et al., 2017). Movies showing the *parS*-ParB:GFP signals detection *in live* meristematic or elongated cells can be find as supplementary data (Suppl. Movies 1 and 2). Altogether, our data demonstrate that the ANCHOR system is suitable for live-cell imaging *in planta.*

Studying chromosome mobility using the ANCHOR system

It is now clear that higher-order organisation of the chromatin exerts an important influence on genomic function during cell differentiation (Arai et al., 2017). For instance, in *Arabidopsis thaliana*, histone exchange dynamics was shown to decrease gradually as cells progressively differentiate (Rosa et al., 2013). However, how chromosomes and the chromatin fibre move during cell differentiation is not well studied in plants. We took advantage of our ANCHOR DNA labelling system to monitor chromatin mobility changes upon cell differentiation in the T2F line. In particular, we measured mobility of *parS*-ParB:GFP *foci* in meristematic and differentiated cells from the root epidermis (Figure 5A) through live-cell imaging using confocal microscopy, and quantified the mobility using mean square displacement (MSD) analysis (Meschichi and Rosa, 2021). Interestingly, the chromatin mobility on meristematic cells was higher than in differentiated cells (Figure 5B, Suppl. Movies 1 and 2). These differences were statistically significant as shown by a much higher radius of constraint (Figure 5C). These results may support the idea that the chromatin in undifferentiated cells holds a more dynamic conformation (Rosa et al., 2013; Arai et al., 2017; Meshorer et al., 2006). However, additional experiments would be required to further validate the biological relevance of this result.

Because until now, single-locus dynamics in plants was mostly possible through the use of the *lacO*/LacI system (Figure 5D) we thought to compare chromatin mobility in meristematic cells using the ANCHOR and the *lacO*/LacI systems. Interestingly, both methods revealed a very similar MSD curve. Indeed, a MSD curve where the maximum values asymptotically reach a plateau, indicates that chromatin moves in a subdiffusive manner, which is typical for chromosomal loci tracked in interphase nuclei (Seeber et al., 2018). Additionally, the curves resulted in comparable measurements of radius of constraint (Figure 5E,F), meaning that the chromatin environment for these two insertion lines may be similar. While comparison with additional lines with different chromosomal locations would be interesting, the results presented here illustrate that the ANCHOR system can be used to monitor single-locus and is suitable to study chromosome organisation and dynamics in plants.

DISCUSSION AND PERSPECTIVES

In this manuscript, we describe a novel method to monitor a single-copy locus i*n planta*. In comparison with existing strategies, the advantage of the ANCHOR system is the absence of repeated elements in the target sequence. This aspect is especially important in plants due to the existence of plant-specific silencing systems (Watanabe et al., 2005; Grob and Grossniklaus, 2019; Matzke et al., 2015). *ParS* sequence is indeed only 1 kb-long and could potentially be shorten to 200 bp (NeoVirtech, personal communication). In addition, several reports in yeast and animal cells have already demonstrated the innocuity of the ANCHOR system to endogenous processes such as transcription and replication (Germier et al., 2018). This particularity makes the ANCHOR system very suitable to monitor single-copy genes in its native genomic environment. In this study, ANCHOR lines were generated by T-DNA insertion. Five out of eight independent lines showed strong ANCHOR signals. This could indicate that ANCHOR insertion site is important to be functional. However, we cannot conclude whether or not the ANCHOR system

is suitable to monitor a genomic locus located in a heterochromatic environment. Absence of *parS*-ParB:GFP *foci* could indeed be a consequence of a lack of ParB:GFP expression, which do not mean that *ParS* accessibility is compromised. Have a separate transgene for parB:GFP expression and *parS* detection would be necessary to address this point. In addition, T-DNA transgenes and Agrobacterium-directed transformation can be a source of genomic and epigenomic instability, both in *cis* and in *trans* (Rajeevkumar et al., 2015). Moreover, they can also modify the nuclear architecture of their insertion site (Grob and Grossniklaus, 2019). To specifically monitor dynamics of selected single loci, the *parS* sequence would need to be inserted at a precise position within the desired locus. A recent approach that combine CRISPR-Cas9 technology and a homologous recombination-donor cassette can generate knock-in *Arabidopsis thaliana* plants (Wolter et al., 2018; Miki et al., 2018; Merker et al., 2020). The implementation of the *parS* knock-in strategy will really improve the innocuity of this approach on the local chromatin state and should strongly reduce any bias on its nuclear positioning.

Another advantage of the ANCHOR approach is the possibility to use simultaneously different combination of *parS*-ParB. ParB binding on *parS* sequence is indeed species-specific and several combinations have successfully been used separately or simultaneously so far. In this study, we used a specific *parS*-ParB , but additional specific combination could be used. In theory, up to three combinations could be used simultaneously (Saad et al., 2014, NeoVirTech peronnal communication), although an important preliminary work would be required for plant material preparation. For instance, two alleles from the same gene could be differentially labelled to monitor their potential associations while being expressed or silenced. This is an important question since previous observations suggest that allele aggregation could participate in gene transcriptional regulation (Rosa et al., 2013). These colour combinations could also be used to follow the distance of two proximal regions during DNA repair for example, as already shown in yeast (Saad et al., 2014) or to label borders of a genomic regions that can undergo different chromatin states during stress or development. This system will provide a useful tool to study the spatial organisation and the dynamic behavior of chromatin at the single locus level.

Competing interest statement

FG is an employee of NeoVirTech and FG and KB are shareholder of NeoVirTech. NeoVirTech did not have any scientific or financial contribution to this study. No other conflict of interest to declare. ANCHOR system is the property of NeoVirTech SAS, Toulouse, France. Any request of use should be addressed to contact@neovirtech.com.

Data access

The sequencing data presented in this article are not readily available due to proprietary restrictions. The remaining original contributions presented in the study are included in the article/supplementary material, further inquiries can be directed to the corresponding author.

Acknowledgments

We thank Guillaume Moissiard, Christophe Tatout and Aline Probst for fruitful discussions. We thank Chritel Llauro for her help with Nanopore sequencing. We also thank the flow cytometry facility, the microscopic facility, and the sequencing facility of platform BioEnvironnement of Perpignan University Via Domitia (Perpignan, France), as well as the Clermont-Ferrand Imagerie Confocale platform (Clermont-Ferrand, France). We acknowledge Rodolphe Dombey for technical assistance and the imaging facility MRI, member of the national infrastructure France-BioImaging infrastructure supported by the French National Research Agency (ANR-10-INBS-04, «Investments for the future»). We thank Marion Orsucci for the help with the statistical

analysis.FP was supported by the Agence Nationale de la Recherche (ANR), JCJC NucleoReg (ANR-15-CE12-0013-01) and by the French Laboratory of Excellence project TULIP (ANR-10-LABX-41 and ANR-11-IDEX-0002-02). MI was supported by the French National Research Agency (ANR-15-CE12-0012). M.M. is a member of the European Training Network "EpiDiverse" that receives funding from the European Union Horizon 2020 program under Marie Skłodowska-Curie grant agreement No. 764965. AM and SR were supported by the Swedish Research Council (Vetenskapsrådet) grant number 2018-04101. A.M., M.I., C.T., N.P., S.R. and F.P. are part of the European Cooperation in Science and Technology COST ACTION CA16212 INDEPTH.

Author contributions:

M.I., F.P. and S.R. designed the experiments. A.M., M.I., C.P. and F.P. performed the experiments. A.M., M.I., N.P., S.R. and F.P. analysed the data. S.D., F.G., K.B. and M.M. participated in material preparation or analysing tools. F.P. wrote the paper and S.R. edited the paper. F.P. acquired main funding.

References:

Arai, R., Sugawara, T., Sato, Y., Minakuchi, Y., Toyoda, A., Nabeshima, K., Kimura, H., and Kimura, A. (2017). Reduction in chromosome mobility accompanies nuclear organization during early embryogenesis in Caenorhabditis elegans. Sci Rep **7**: 3631.

Blanco-Rodriguez, G., Gazi, A., Monel, B., Frabetti, S., Scoca, V., Mueller, F., Schwartz, O., Krijnse-Locker, J., Charneau, P., and Di Nunzio, F. (2020). Remodeling of the Core Leads HIV-1 Preintegration Complex into the Nucleus of Human Lymphocytes. J Virol **94**.

Clough, S.J. and Bent, A.F. (1998). Floral dip: a simplified method for Agrobacterium-mediated transformation of Arabidopsis thaliana. Plant J **16**: 735–743.

Dubarry, N., Pasta, F., and Lane, D. (2006). ParABS systems of the four replicons of Burkholderia cenocepacia: new chromosome centromeres confer partition specificity. Journal of bacteriology **188**: 1489–1496.

Dumur, T., Duncan, S., Graumann, K., Desset, S., Randall, R.S., Scheid, O.M., Prodanov, D., Tatout, C., and Baroux, C. (2019). Probing the 3D architecture of the plant nucleus with microscopy approaches: challenges and solutions. Nucleus **10**: 181–212.

Durut, N. et al. (2014). A duplicated NUCLEOLIN gene with antagonistic activity is required for chromatin organization of silent 45S rDNA in Arabidopsis. The Plant cell **26**: 1330–1344.

Earley, K.W., Haag, J.R., Pontes, O., Opper, K., Juehne, T., Song, K., and Pikaard, C.S. (2006). Gateway-compatible vectors for plant functional genomics and proteomics. Plant J **45**: 616–629.

Fang, Y. and Spector, D.L. (2007). Identification of nuclear dicing bodies containing proteins for microRNA biogenesis in living Arabidopsis plants. Current biology : CB **17**: 818–823.

Feng, C.-M., Qiu, Y., Van Buskirk, E.K., Yang, E.J., and Chen, M. (2014). Light-regulated gene repositioning in Arabidopsis. Nature communications **5**: 3027.

Fujimoto, S., Sugano, S.S., Kuwata, K., Osakabe, K., and Matsunaga, S. (2016). Visualization of specific repetitive genomic sequences with fluorescent TALEs in Arabidopsis thaliana. J Exp Bot **67**: 6101–6110.

Funnell, B.E. (2016). ParB Partition Proteins: Complex Formation and Spreading at Bacterial and Plasmid Centromeres. Front Mol Biosci **3**: 44.

Gallardo, F. et al. (2020). Fluorescent Tagged Vaccinia Virus Genome Allows Rapid and Efficient Measurement of Oncolytic Potential and Discovery of Oncolytic Modulators. Biomedicines **8**.

Germier, T., Audibert, S., Kocanova, S., Lane, D., and Bystricky, K. (2018). Real-time imaging of specific genomic loci in eukaryotic cells using the ANCHOR DNA labelling system. Methods **142**: 16–23.

Germier, T., Kocanova, S., Walther, N., Bancaud, A., Shaban, H.A., Sellou, H., Politi, A.Z., Ellenberg, J., Gallardo, F., and Bystricky, K. (2017). Real-Time Imaging of a Single Gene Reveals Transcription-Initiated Local Confinement. Biophys J **113**: 1383–1394.

Grob, S. and Grossniklaus, U. (2019). Invasive DNA elements modify the nuclear architecture of their insertion site by KNOT-linked silencing in Arabidopsis thaliana. Genome Biol **20**: 120.

Hinsberger, A., Graillot, B., Blachère Lopez, C., Juliant, S., Cerutti, M., King, L.A., Possee, R.D., Gallardo, F., and Lopez Ferber, M. (2020). Tracing Baculovirus AcMNPV Infection Using a Real-Time Method Based on ANCHOR(TM) DNA Labeling Technology. Viruses **12**.

Kato, N. and Lam, E. (2003). Chromatin of endoreduplicated pavement cells has greater range of movement than that of diploid guard cells in Arabidopsis thaliana. J Cell Sci **116**: 2195–2201.

Kearse, M. et al. (2012). Geneious Basic: an integrated and extendable desktop software platform for the organization and analysis of sequence data. Bioinformatics **28**: 1647–1649.

Khosravi, S., Dreissig, S., Schindele, P., Wolter, F., Rutten, T., Puchta, H., and Houben, A. (2020). Live-Cell CRISPR Imaging in Plant Cells with a Telomere-Specific Guide RNA. Methods Mol Biol **2166**: 343–356.

Komatsu, T. et al. (2018). In Vivo Labelling of Adenovirus DNA Identifies Chromatin ANCHORing and Biphasic Genome Replication. J Virol **92**.

Lindhout, B.I., Fransz, P., Tessadori, F., Meckel, T., Hooykaas, P.J.J., and van der Zaal, B.J. (2007). Live cell imaging of repetitive DNA sequences via GFP-tagged polydactyl zinc finger proteins. Nucleic Acids Res **35**: e107.

Mariamé, B., Kappler-Gratias, S., Kappler, M., Balor, S., Gallardo, F., and Bystricky, K. (2018). Real-Time Visualization and Quantification of Human Cytomegalovirus Replication in Living Cells Using the ANCHOR DNA Labeling Technology. J Virol **92**.

Matzke, A.J.M., Huettel, B., van der Winden, J., and Matzke, M. (2005). Use of two-color fluorescence-tagged transgenes to study interphase chromosomes in living plants. Plant Physiol **139**: 1586–1596.

Matzke, M.A., Kanno, T., and Matzke, A.J.M. (2015). RNA-Directed DNA Methylation: The Evolution of a Complex Epigenetic Pathway in Flowering Plants. Annu Rev Plant Biol **66**: 243–267.

Merker, L., Schindele, P., and Puchta, H. (2020). Using CRISPR/ttLbCas12a for in planta Gene Targeting in A. thaliana. Curr Protoc Plant Biol **5**: e20117.

Meschichi, A. and Rosa, S. (2021). Visualizing and Measuring Single Locus Dynamics in Arabidopsis thaliana. Methods Mol Biol **2200**: 213–224.

Meshorer, E., Yellajoshula, D., George, E., Scambler, P.J., Brown, D.T., and Misteli, T. (2006). Hyperdynamic plasticity of chromatin proteins in pluripotent embryonic stem cells. Dev Cell **10**: 105–116.

Miki, D., Zhang, W., Zeng, W., Feng, Z., and Zhu, J.-K. (2018). CRISPR/Cas9-mediated gene targeting in Arabidopsis using sequential transformation. Nat Commun **9**: 1967.

Nguyen, H.Q. and Bosco, G. (2015). Gene Positioning Effects on Expression in Eukaryotes. Annu Rev Genet **49**: 627–646.

Picart-Picolo, A. et al. (2020). Large tandem duplications affect gene expression, 3D organization, and plant-pathogen response. Genome Res **30**: 1583–1592.

Pontvianne, F., Blevins, T., Chandrasekhara, C., Feng, W., Stroud, H., Jacobsen, S.E., Michaels, S.D., and Pikaard, C.S. (2012). Histone methyltransferases regulating rRNA gene dose and dosage control in Arabidopsis. Genes & development **26**: 945–957.

Pontvianne, F., Boyer-Clavel, M., and Saez-Vasquez, J. (2016). Fluorescence-Activated Nucleolus Sorting in Arabidopsis. Methods in molecular biology (Clifton, N.J.) **1455**: 203–211.

Pontvianne, F. and Grob, S. (2020). Three-dimensional nuclear organization in Arabidopsis thaliana. J Plant Res **133**: 479–488.

Pontvianne, F. and Liu, C. (2019). Chromatin domains in space and their functional implications. Curr Opin Plant Biol **54**: 1–10.

Rajeevkumar, S., Anunanthini, P., and Sathishkumar, R. (2015). Epigenetic silencing in

transgenic plants. Front Plant Sci **6**: 693.
Rosa, S., De Lucia, F., Mylne, J.S., Zhu, D., Ohmido, N., Pendle, A., Kato, N., Shaw, P., and Dean, C. (2013). Physical clustering of FLC alleles during Polycomb-mediated epigenetic silencing in vernalization. Genes & development **27**: 1845–1850.
Saad, H., Gallardo, F., Dalvai, M., Tanguy-le-Gac, N., Lane, D., and Bystricky, K. (2014). DNA dynamics during early double-strand break processing revealed by non-intrusive imaging of living cells. PLoS genetics **10**: e1004187.
Santos, A.P., Gaudin, V., Mozgová, I., Pontvianne, F., Schubert, D., Tek, A.L., Dvořáčková, M., Liu, C., Fransz, P., Rosa, S., and Farrona, S. (2020). Tiding-up the plant nuclear space: domains, function and dynamics. J Exp Bot.
Seeber, A., Hauer, M.H., and Gasser, S.M. (2018). Chromosome Dynamics in Response to DNA Damage. Annu Rev Genet **52**: 295–319.
Sequeira-Mendes, J., Araguez, I., Peiro, R., Mendez-Giraldez, R., Zhang, X., Jacobsen, S.E., Bastolla, U., and Gutierrez, C. (2014). The Functional Topography of the Arabidopsis Genome Is Organized in a Reduced Number of Linear Motifs of Chromatin States. The Plant cell **26**: 2351–2366.
Shaban, H.A. and Seeber, A. (2020). Monitoring global chromatin dynamics in response to DNA damage. Mutat Res **821**: 111707.
Watanabe, K., Pecinka, A., Meister, A., Schubert, I., and Lam, E. (2005). DNA hypomethylation reduces homologous pairing of inserted tandem repeat arrays in somatic nuclei of Arabidopsis thaliana. Plant J **44**: 531–540.
Wolter, F., Klemm, J., and Puchta, H. (2018). Efficient in planta gene targeting in Arabidopsis using egg cell-specific expression of the Cas9 nuclease of Staphylococcus aureus. Plant J **94**: 735–746.
Yelagandula, R. et al. (2014). The histone variant H2A.W defines heterochromatin and promotes chromatin condensation in Arabidopsis. Cell **158**: 98–109.

Figures legend

Figure 1 : Description of the ANCHOR system i*n planta*

A. Schematic representation of the ANCHOR system. ParB proteins fused to GFP can directly bound to *parS* sequence as a dimer. *parS*-ParB interactions provoke a conformational change in ParB proteins that induce their oligomerization along the flanking genomic region. **B.** Cassette used to transform *Arabidopsis thaliana* Col-0 plants to test the ANCHOR system *in planta.* A strong and ubiquitous promoter is used to express the ParB protein fused to GFP and three FLAG tags. After a Terminator sequence, a 1.5 kb-long spacer sequence has been added to separate the ParB:GFP open reading frame and the 1 kb-long *parS* sequence. Detection of a *parS*-ParB:GFP focus (Green) in an isolated leaf nucleus **(C**) and in fixed root tissues (**D**) of *A. thaliana* plants containing the ANCHOR cassette described in **B**. Nuclear DNA is labelled with DAPI (blue). Bar = 5 µm. **E**. Position of the transgene in the ANCHOR line T2F in the Arabidopsis genome using Nanopore sequencing. The transgene presented in **B** is inserted on chromosome 5, position 23.675.998 pb.

Figure 2 : Detection of *parS*-ParB foci in cells with different ploidy levels and after immunolocalization experiments"

A. Detection of *parS*-ParB:GFP foci (Green) in fixed and sorted nuclei according to their ploidy levels by Fluorescent-Assisted Cell Sorting (FACS). Nuclear DNA is labeled with DAPI (grey). Enlarged view of the *parS*-ParB:GFP foci are presented to facilitate signal visualisation. Bar = 1 µm. **B-C**. Detection of *parS*-ParB:GFP foci (Green) and post-translationally modified histones (red) in fixed and isolated nuclei *from A. thaliana* Col-0 plants T2F. The image correspond to a confocal 2D stack. Nuclear DNA is labeled with DAPI (grey). Trimethylated H3K27 signals are shown in the panel **B**, while acetylated

505 H3 are shown in the panel **C**. Enlarged views of the *parS*-ParB:GFP foci are presented to facilitate
506 signal visualization. Bar = 2 μm.
507
508 **Figure 3: ANCHOR system is suitable to monitor a single-copy locus in live and in different tissues**
509 Schematic representation of an *Arabidopsis thaliana* plant illustrating the different tissues in
510 which *parS*-ParB: GFP signals have been detected by live-cell imaging. ParB:GFP signals are in
511 green and H2A.W:RFP is shown in red. Scale bars = 5 μm.
512
513 **Figure 4: Monitoring *parS*-ParB:GFP in live during mitosis or during a time-course**
514 **A**. Detection of *parS*-ParB:GFP foci (green) and H2A.W:RFP (red) in mitotic cells. Scale Bars = 5 μm
515 **B**. ANCHOR system enables time-lapse tracking of a single-locus in live roots by confocal imaging.
516 Time-lapse acquisition of *parS*-ParB:GFP signals (grey) in an endoreplicated root cell over 5 min.
517
518 **Figure 5: Analysing chromatin mobility using the ANCHOR system.**
519 **A**. Representative images of ParB-*parS* line in meristematic (upper panel) and differentiation zone
520 (bottom panel) showing nuclear signal with spots (cyan). Propidium Iodide (PI) staining (ma-
521 genta). Bars = 10 µm. **B.** MSD analysis for ParB-*parS* lines based on time-lapse experiments of nu-
522 clei in the meristematic and differentiated zone. 3D stacks were taken at 6 sec intervals for 5min.
523 Values represent mean ± SEM from 54 and 9 cells, respectively. **C**. Calculated radius of constraint
524 for MSD curves depicted in B. Values represent means ± SEM. Student's *t* test, ***P < 0.001. **D.**
525 Representative image of *lacO*/LacI line in meristematic region showing nuclear signal with spots
526 (cyan). Propidium Iodide (PI) staining (magenta). Bar = 10 µm. **E.** MSD analysis for *lacO*/LacI and
527 ParB-*parS* lines based on time lapse experiment of nuclei in the meristematic zone. Values repre-
528 sent means ± SEM from 116 and 54 cells, respectively. **F.** Calculated radius of constraint for MSD
529 curves depicted in E. Values represent means ± SEM.
530
531
532 **Supplemental figures legend**
533
534 **Figure S1: Chromatin states flanking the insertion site in T2F ANCHOR line.**
535 **A.** Snapshot of the chromatin states enriched in the region flanking the transgene insertion site in
536 the line T2F (https://jbrowse.arabidopsis.org/). **B.** Histogram representing the relative enrichment
537 of each chromatin state in the 5 kb upstream and downstream region of the transgene insertion
538 site in the line T2F.
539
540 **Figure S2 : Detection of *parS*-ParB foci in cells with different ploidy levels**
541 Detection of *parS*-ParB:GFP foci (Green) in fixed and sorted nuclei according to their ploidy levels
542 by Fluorescent-Assisted Cell Sorting (FACS). Nuclear DNA is labeled with DAPI (grey).
543
544 **Figure S3: Pollen and trichome cell.**
545 Confocal images of the *parS*-ParB:GFP signal in a trichome cell (top panels) or in pollen cells (bottom
546 panels). Images on the right are saturated to show the trichome contour or the pollen grains.
547
548 **Figure S4: Co-localization of *parS*-ParB foci with H3Ac and H3K27me3 marks**
549 Detection of *parS*-ParB:GFP foci (Green) and post-translationally modified histones (red) in fixed
550 and isolated nuclei *from A. thaliana* Col-0 plants T2F. Nuclear DNA is labeled with DAPI (grey). Tri-
551 methylated H3K27 signals are shown in the panel **A**, while acetylated H3 are shown in the panel **B.**
552 **C** and **D** panels show the relative intensity of each signal.
553

Figure 1

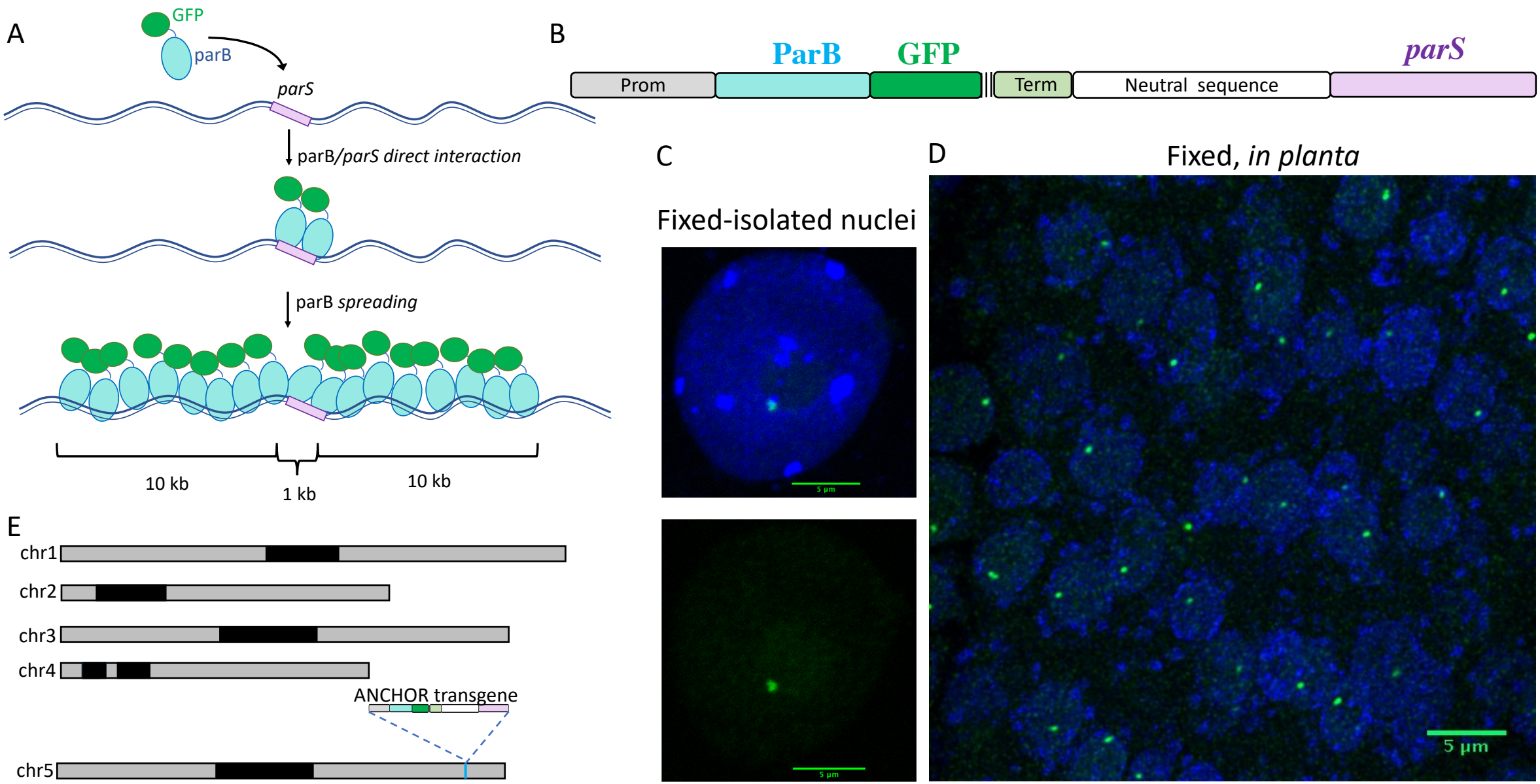
A
GFP
parB
parS
parB/parS direct interaction
parB spreading
10 kb
1 kb
10 kb
B
ParB
GFP
parS
Prom
Term
Neutral sequence
C
Fixed-isolated nuclei
5 µm
5 µm
D
Fixed, in planta
5 µm
E
chr1
chr2
chr3
chr4
ANCHOR transgene
chr5

Figure 2

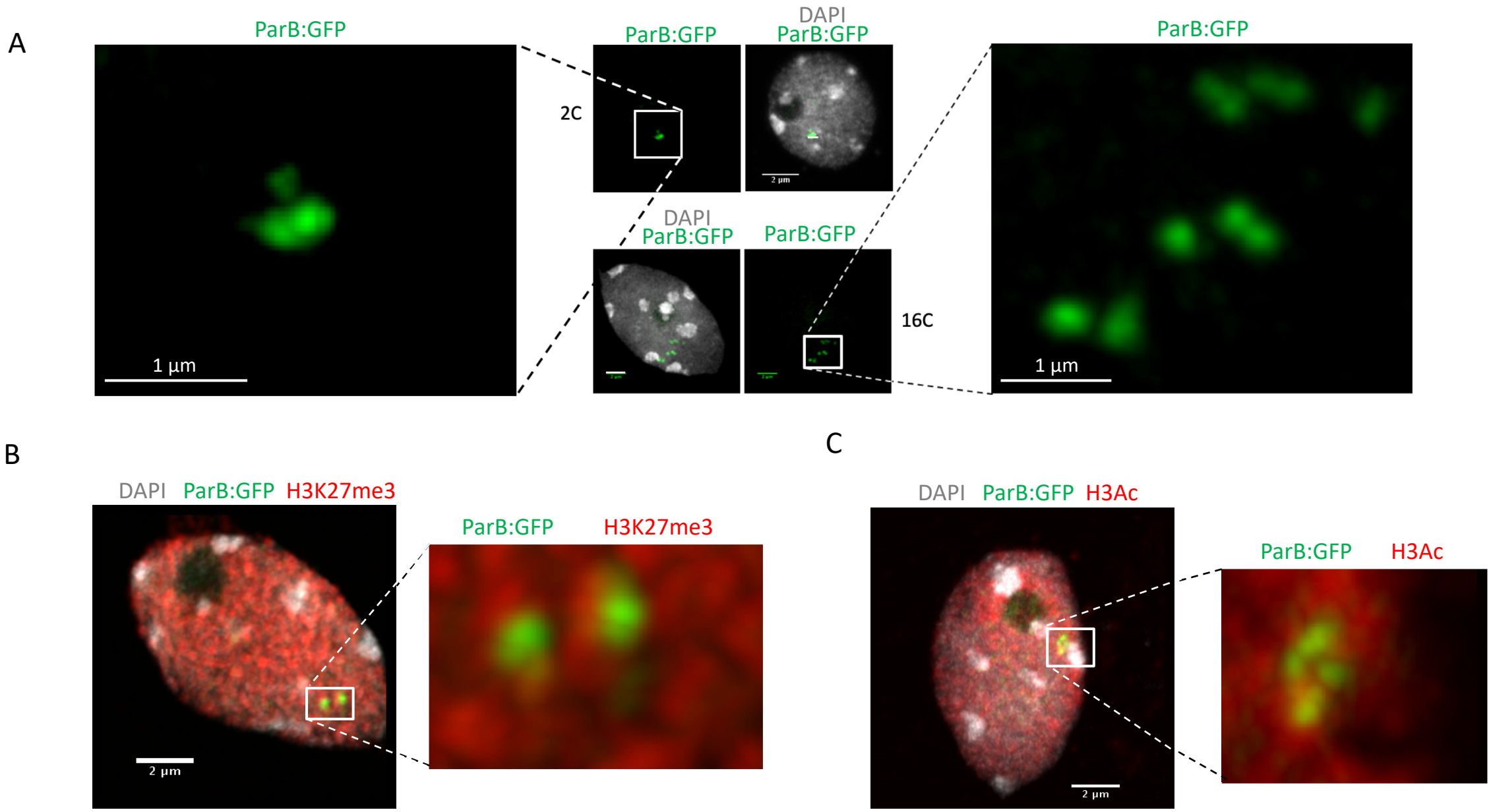
A
ParB:GFP
1 µm
ParB:GFP
2C
DAPI
ParB:GFP
2 µm
DAPI
ParB:GFP
ParB:GFP
16C
ParB:GFP
1 µm
B
DAPI ParB:GFP H3K27me3
2 µm
ParB:GFP H3K27me3
C
DAPI ParB:GFP H3Ac
2 µm
ParB:GFP H3Ac

Figure 3

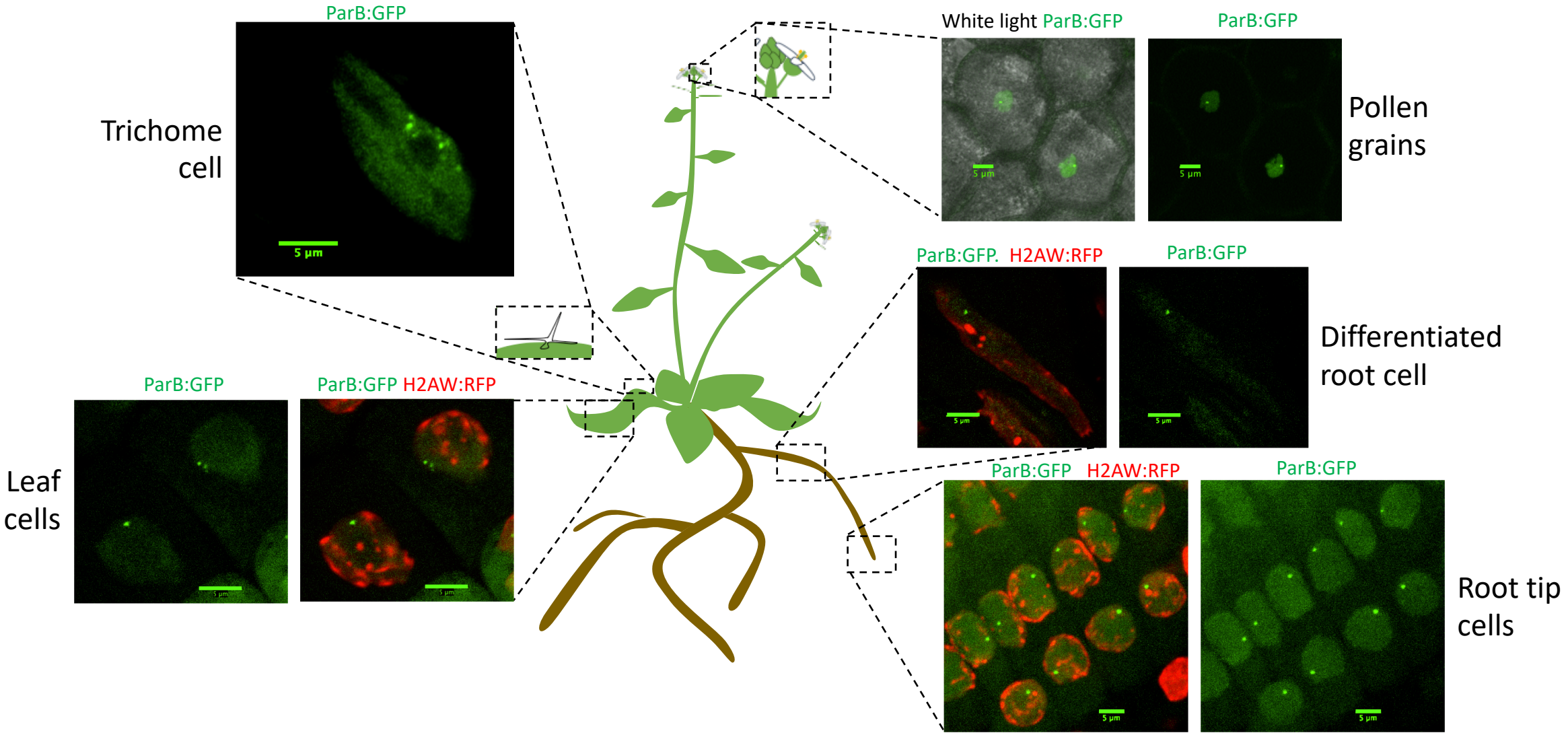
ParB:GFP
Trichome cell
5 µm
White light ParB:GFP
ParB:GFP
Pollen grains
ParB:GFP. H2AW:RFP
ParB:GFP
Differentiated root cell
ParB:GFP
ParB:GFP H2AW:RFP
Leaf cells
ParB:GFP H2AW:RFP
ParB:GFP
Root tip cells

Figure 4

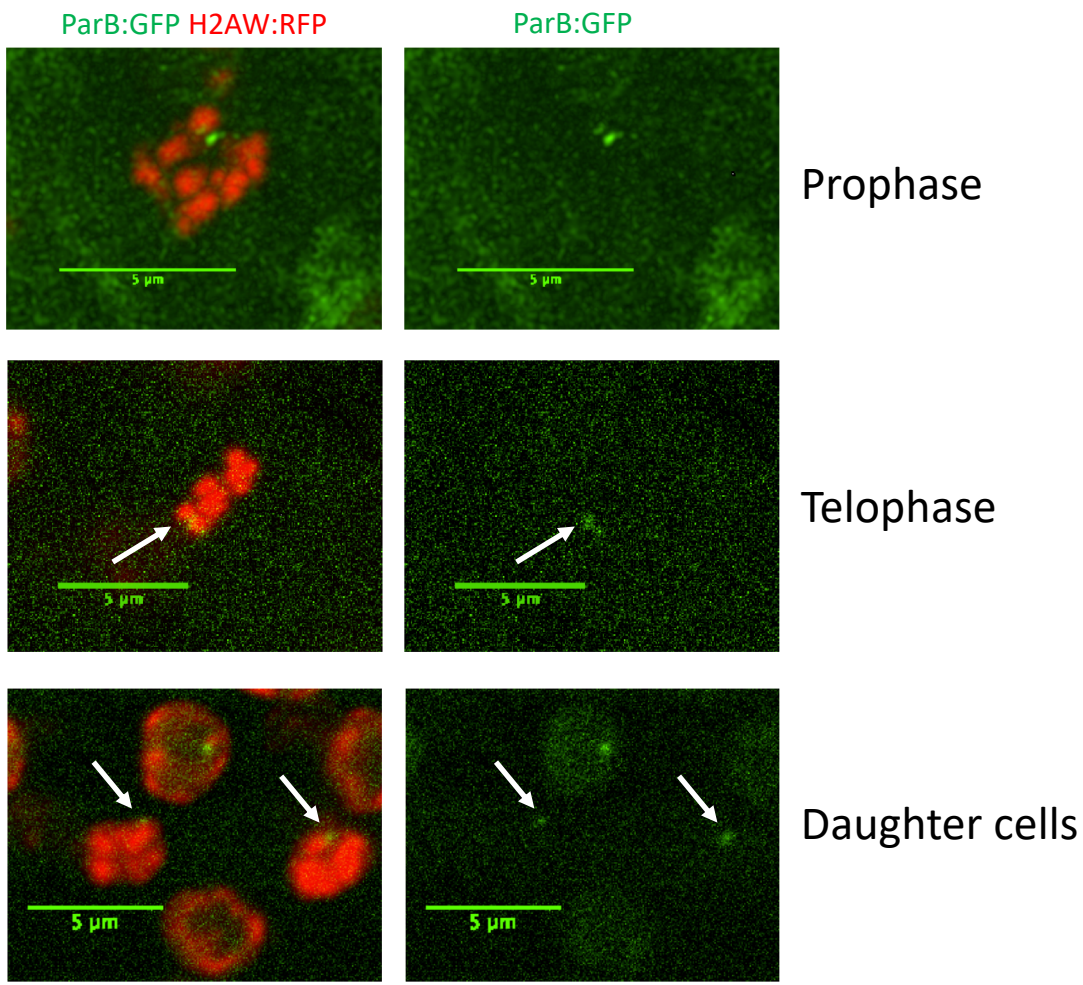
A
ParB:GFP H2AW:RFP
ParB:GFP
Prophase
Telophase
Daughter cells
5 µm

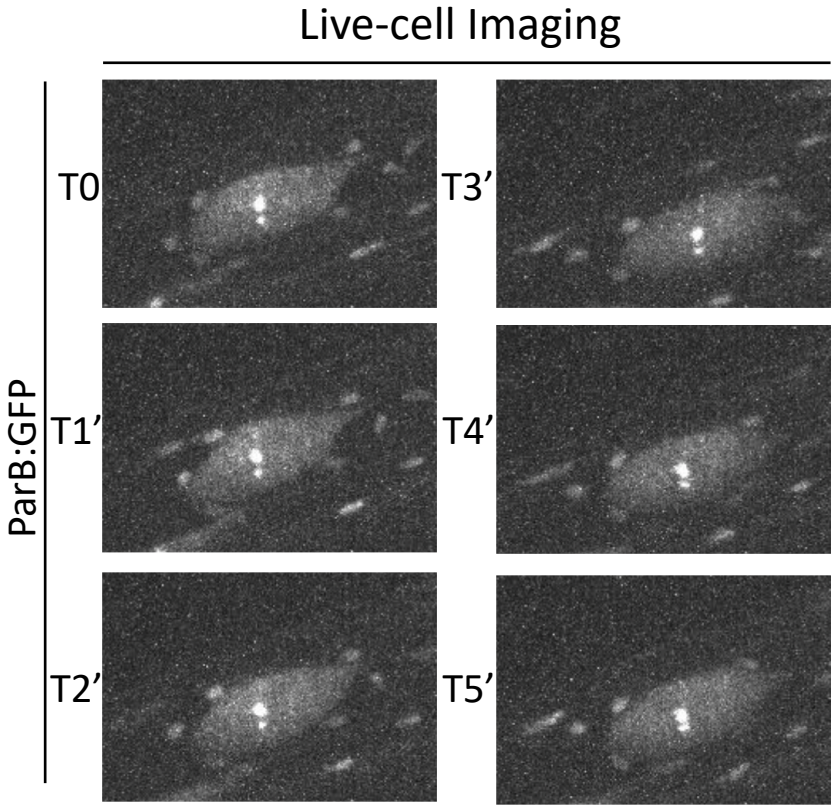
B
Live-cell Imaging
ParB:GFP
T0
T1'
T2'
T3'
T4'
T5'

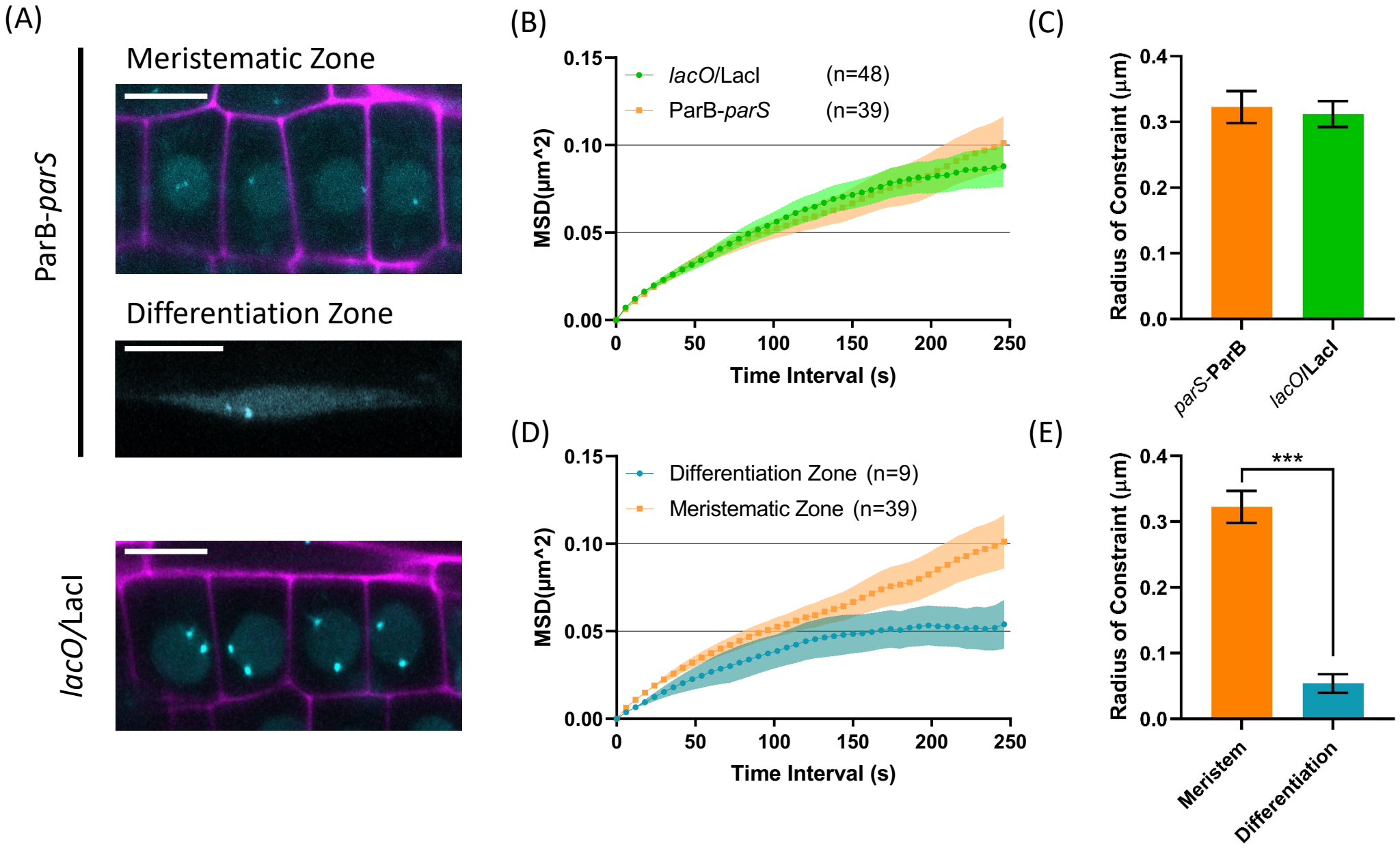
(A)
Meristematic Zone
ParB-parS
Differentiation Zone
lacO/LacI
(B)
lacO/LacI (n=48)
ParB-parS (n=39)
MSD(µm^2)
0.15
0.10
0.05
0.00
0
50
100
150
200
250
Time Interval (s)
(C)
Radius of Constraint (µm)
0.4
0.3
0.2
0.1
0.0
parS-ParB
lacO/LacI
(D)
Differentiation Zone (n=9)
Meristematic Zone (n=39)
MSD(µm^2)
0.15
0.10
0.05
0.00
0
50
100
150
200
250
Time Interval (s)
(E)
Radius of Constraint (µm)
***
0.4
0.3
0.2
0.1
0.0
Meristem
Differentiation

Figure S1

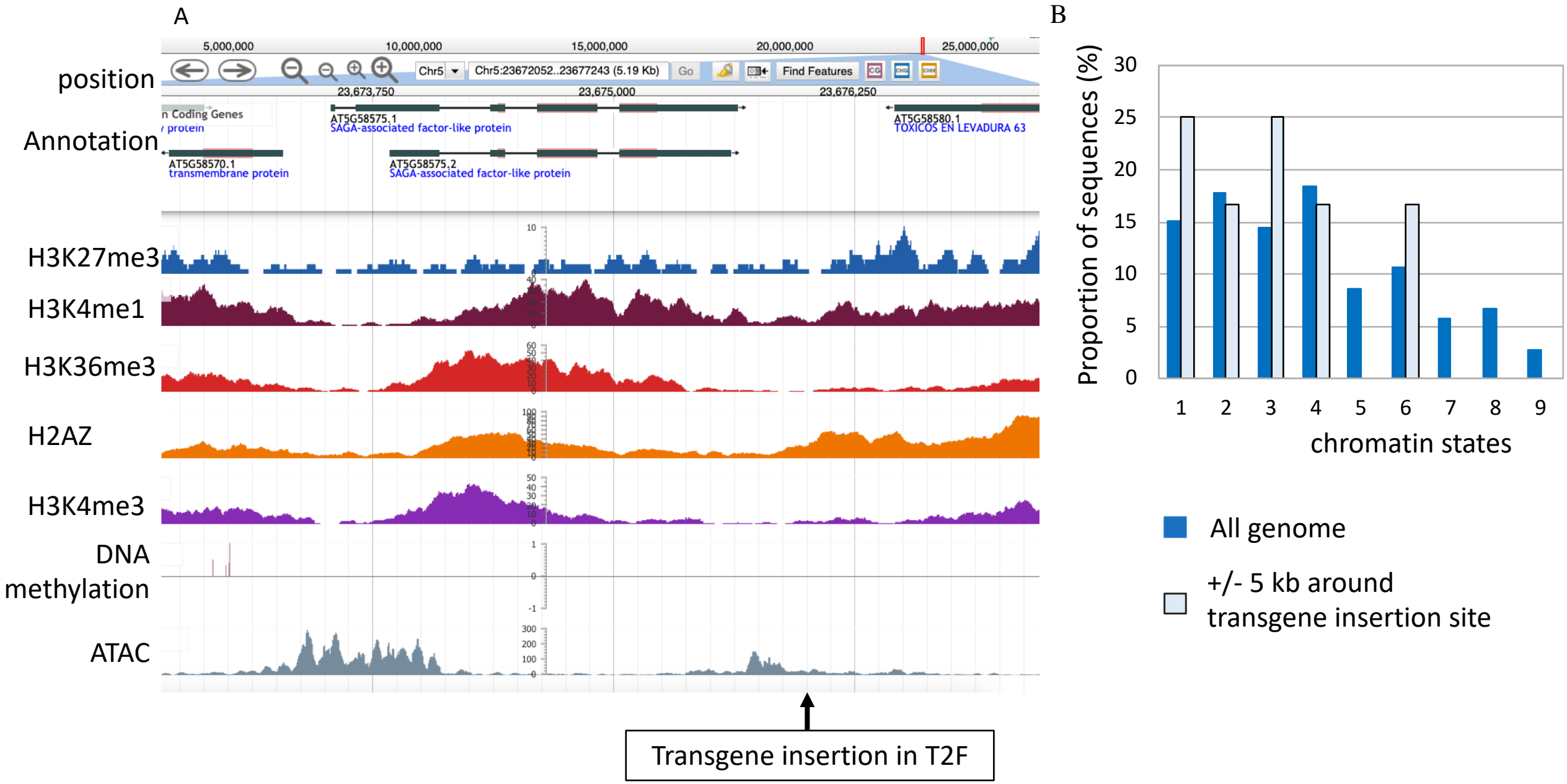
A
position
Annotation
5,000,000
10,000,000
15,000,000
20,000,000
25,000,000
Chr5
Chr5:23672052..23677243 (5.19 Kb)
Go
Find Features
23,673,750
23,675,000
23,676,250
AT5G58575.1
SAGA-associated factor-like protein
AT5G58580.1
TOXICOS EN LEVADURA 63
AT5G58570.1
transmembrane protein
AT5G58575.2
SAGA-associated factor-like protein
H3K27me3
H3K4me1
H3K36me3
H2AZ
H3K4me3
DNA methylation
ATAC
Transgene insertion in T2F
B
Proportion of sequences (%)
30
25
20
15
10
5
0
1
2
3
4
5
6
7
8
9
chromatin states
All genome
+/- 5 kb around transgene insertion site

Figure S2

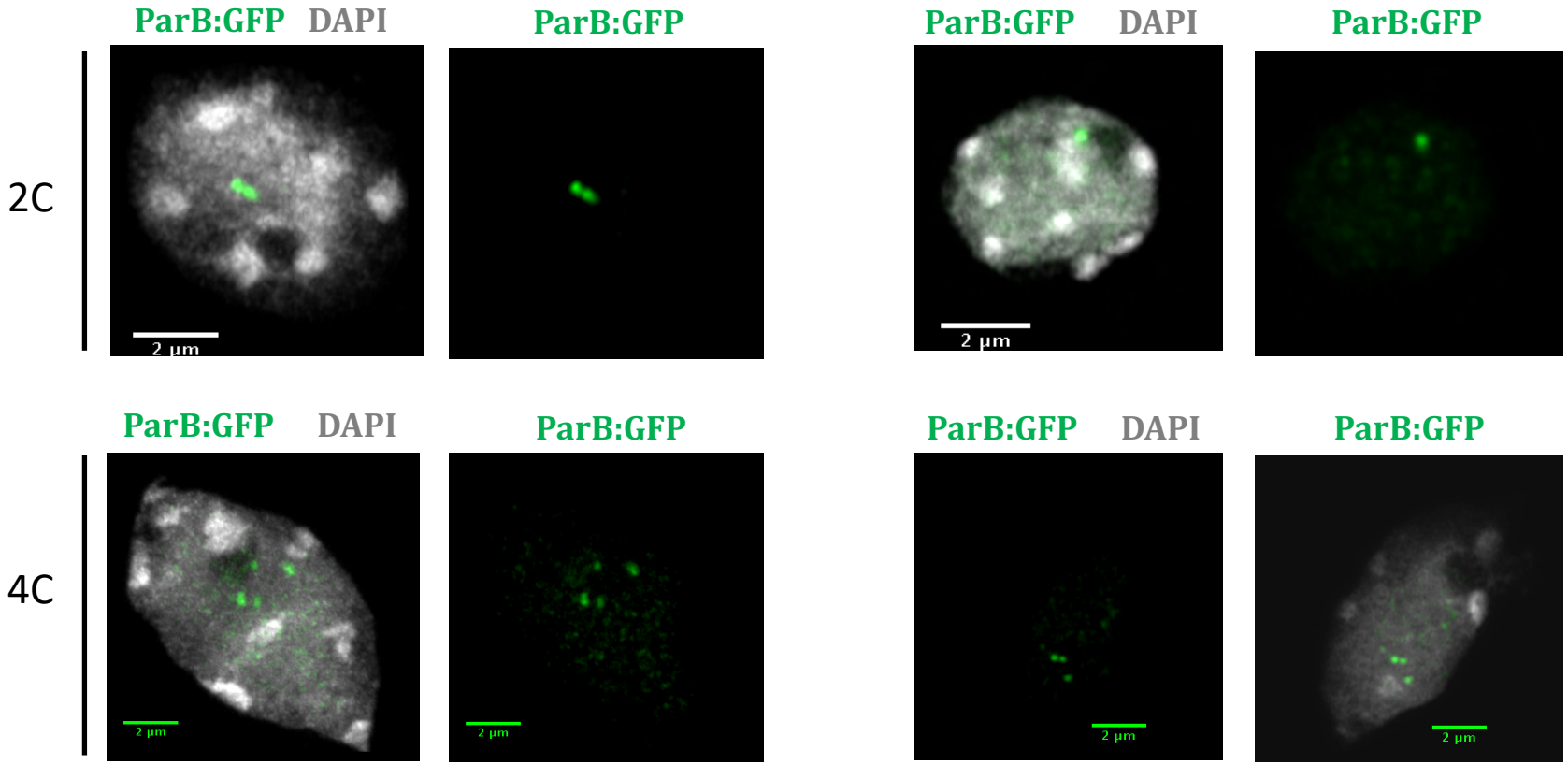
ParB:GFP DAPI
ParB:GFP
ParB:GFP DAPI
ParB:GFP
2C
2 µm
2 µm
ParB:GFP DAPI
ParB:GFP
ParB:GFP DAPI
ParB:GFP
4C
2 µm
2 µm
2 µm
2 µm

Figure S3

Trichome cell

ParB:GFP

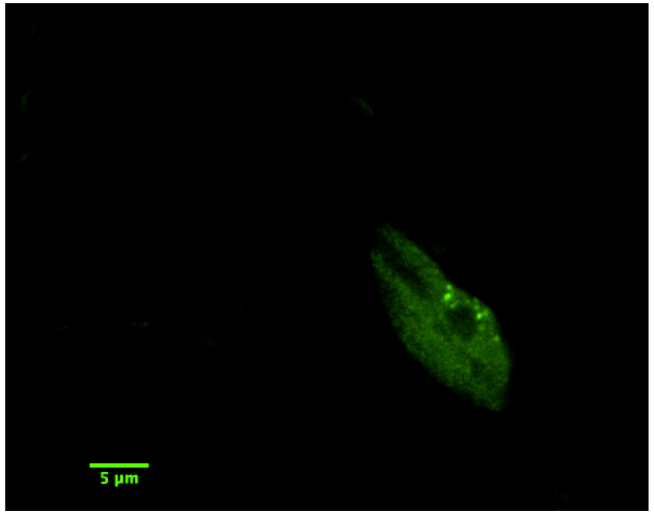

ParB:GFP (saturated)

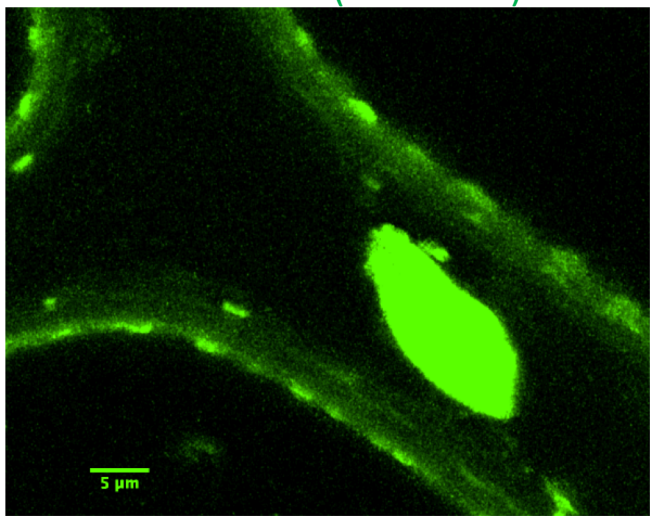

Pollen cells

ParB:GFP

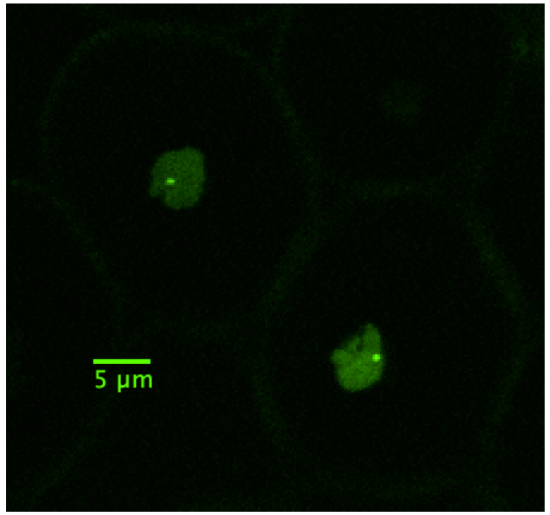

ParB:GFP (saturated)

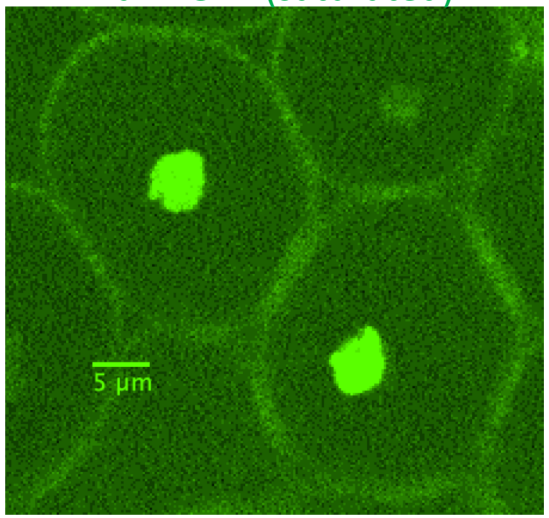

Figure S4

A

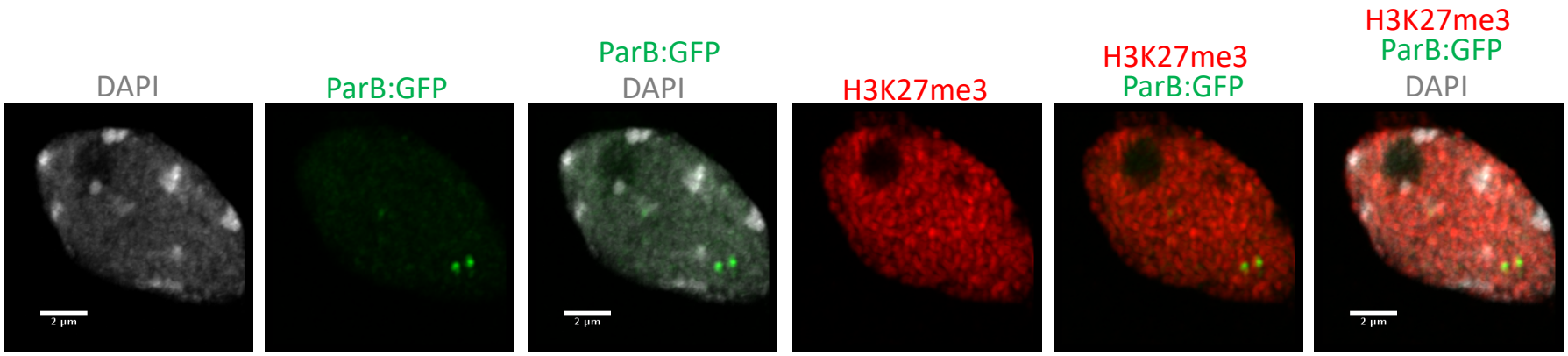

B

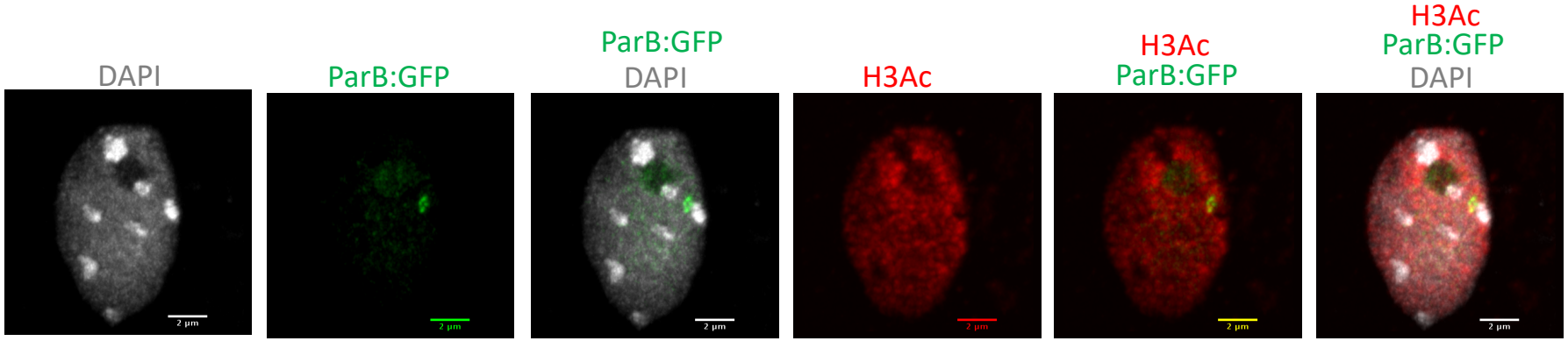

C

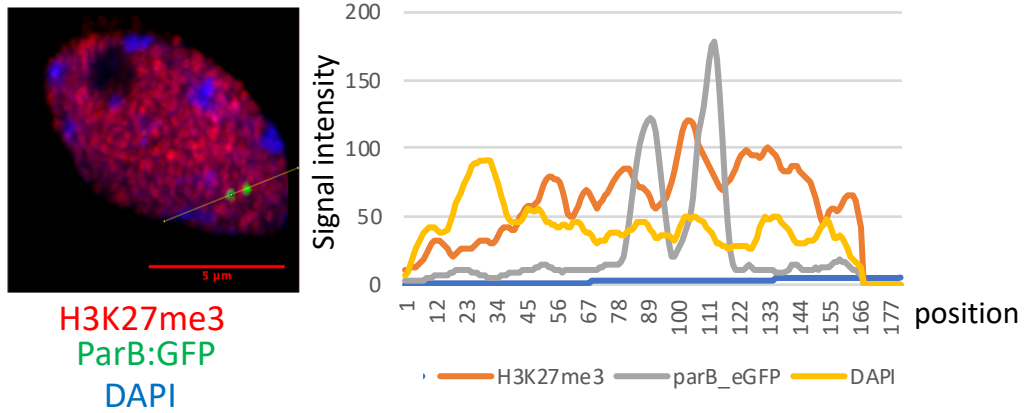

D